ACS APPLIED ENERGY MATERIALS
Cite This: ACS Appl. Energy Mater. 2019, 2, 7244−7255
Article
www.acsaem.org

Facile Synthesis of a Tin Oxide-Carbon Composite Lithium-Ion Battery Anode with High Capacity Retention

Jason A. Weeks,[†] Ho-Hyun Sun,[‡] Hrishikesh S. Srinivasan,[‡] James N. Burrow,[‡] Joseph V. Guerrera,[†] Melissa L. Meyerson,[†] Andrei Dolocan,[§] Adam Heller,[‡] and C. Buddie Mullins*[,†,‡]

[†]Department of Chemistry, [‡]Department of Chemical Engineering, and [§]Texas Materials Institute, The University of Texas at Austin, Austin, Texas 78712, United States

Supporting Information

ABSTRACT: A tin oxide-carbon composite (SnO_x-C) was fabricated as a candidate for use as an anode in lithium-ion batteries through the pyrolysis of a ditin citrate precursor. The simultaneous formation of tin oxide and semigraphitized carbon via a facile, solid-state pyrolysis yielded a composite containing tin oxide nanocrystals surrounded by a framework of flexible, porous carbon. Fabrication of tin oxide nanoparticles encased in semigraphitized carbon, led to the enhanced reversibility of Li_2O formation, prevented the aggregation of tin during lithiation and suppressed particle fracturing during cycling. The resulting SnO_x-C composite exhibited an exceptional electrochemical performance as an anode material candidate for lithium-ion batteries with an initial capacity of 541 mAh g^{-1} and 80.6% capacity retention over 400 cycles at a high current density of 900 mA g^{-1} (1C). Lower current density studies [450 mA g^{-1} (C/2)] have shown the material to have an initial capacity of 667 mAh g^{-1} with 88.7% capacity retention over 400 cycles, whereas a current density of 180 mA g^{-1} (C/5) gave a capacity of 710 mAh g^{-1} with 88.8% capacity retention over 400 cycles. Through a systematic analysis involving X-ray diffraction, X-ray photoelectron spectroscopy, Raman spectroscopy, cyclic voltammetry, cross-sectional analysis, and post-mortem analysis, we examine how the architecture and composition of the SnO_x-C material leads to a high capacity retention tin oxide-carbon composite anode for lithium-ion batteries.

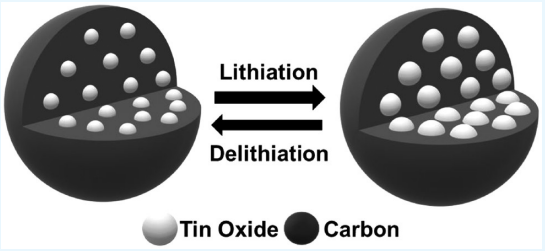

KEYWORDS: *Tin oxide, lithium-ion battery, anode, composite, conversion*

INTRODUCTION

As society narrows its focus on energy production through renewable energy sources, the demand for energy storage and transport dramatically increases. Although more environmentally benign, these renewable sources of energy are often intermittent, requiring storage for later use and transport to the consumers.[1,2] In this regard, lithium-ion batteries (LIBs) are the preferred energy storage method in small grid and consumer systems due to their high power and energy densities. However, the LIB anode technology has remained rather stagnant over the past three decades due to graphite's robustness and exceptional cycle-life.[1,3] The down-side of graphite is its relatively low theoretical capacity (372 mAh/g).[3] As the demand for greater processing power in consumer electronics grows and electric vehicles become more predominant in society, the demand for greater energy density will become more imperative, as well as the maintenance of the current technology's price point and lifetime.[2]

In efforts to increase the energy density in LIBs, researchers have investigated the use of higher capacity anode materials that store Li through alloying or conversion reactions.[4−7] Tin oxide is a particularly alluring anode material due to its high environmental abundance, low-price point, and nonhazardous properties.[5,8] Furthermore, tin oxide has superior lithium uptake potential compared to graphite with approximately four times the gravimetric capacity (SnO_2 = 1494 mA g^{-1}, SnO = 1273 mA g^{-1}),[7,9−11] which is derived from the combination of tin oxide's conversion and alloying reactions with lithium (eqs 1−3).[9,12] Even though this material has been shown to display high gravimetric capacity, outstanding volumetric energy density, and adequate Coulombic efficiencies, there is a continuing effort to improve the cycle life of the material. The reasons for cycle life degradation are ascribed to (1) severe volumetric expansion (~300%),[7,9,11,13] (2) the irreversibility of lithium oxide (Li_2O) formation,[14−19] and (3) aggregation of tin particles during cycling.[9,14] The large volumetric expansion is primarily due to the formation of Li_2O (eqs 1 and 2) and the high degree of lithiation per atom of tin (eq 3) which is known to cause fracturing of the particles. Particle fracture leads to (1) consumption of electrolyte through the formation of fresh solid electrolyte interface (SEI) on newly exposed tin oxide and (2) a potential electrical disconnect from the current collector.[20−22] The low reversibility for the formation of Li_2O has been attributed to the disruption of the Li_2O matrix via cycling.[9,10] Another hindrance is that metallic tin particles are notorious for

Received: June 17, 2019
Accepted: October 3, 2019
Published: October 3, 2019

DOI: 10.1021/acsaem.9b01205
ACS Appl. Energy Mater. 2019, 2, 7244−7255

Scheme 1. Comparison of SnO_x-C Lithiation/Delithiation versus Unsupported Tin Oxide Particle Lithiation/Delithiation

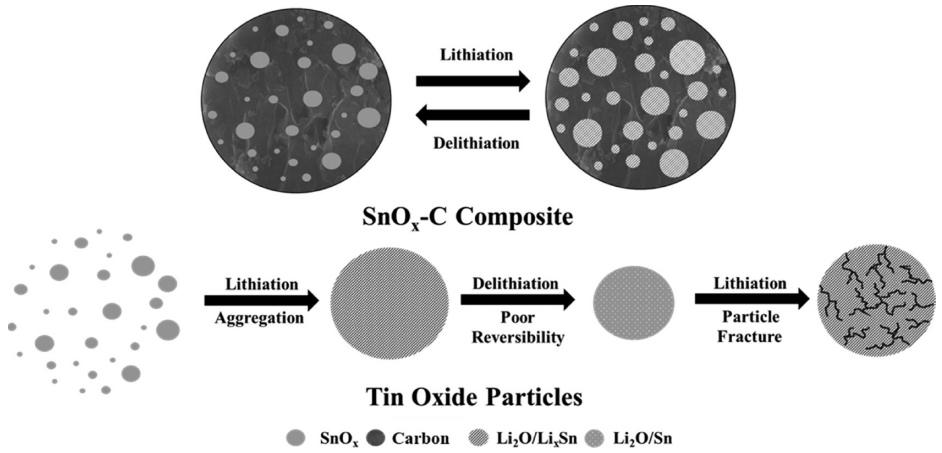

clustering during galvanostatic cycling.[9,14] The aggregation of tin particles during cycling disturbs the newly formed Li_2O matrix and reduces the interactions between the tin and Li_2O matrices.[10] These effects cause the formation of Li_2O to be nearly irreversible in many electrochemical systems.[14−19]

$$SnO_2 + 2Li^+ + 2e^- \rightarrow Li_2O + SnO \quad (1)$$

$$SnO + 2Li^+ + 2e^- \rightarrow Li_2O + Sn \quad (2)$$

$$Sn + xLi^+ + xe^- \rightarrow Li_xSn\ (0 \leq x \leq 4.4) \quad (3)$$

Numerous groups have attempted to improve the cyclability of tin oxide, primarily by employing methods that counteract the large volumetric expansion caused by lithiation. Some of the employed technologies are hollow nanospheres,[23−26] electrospun tin oxide nanofibers,[18,27,28] yolk-type composites,[11,16,17] anchoring tin oxide nanoparticles to rGO/GO,[29] and synthesis of carbon-coated composites.[14,19,30,31] Despite these methods demonstrating improvements in the cycle-life, when compared to simple tin oxide nanoparticles[32,33] these methods are often industrially unviable due to the specialized, nonscalable, and/or high energy synthetic techniques required for fabrication. For tin oxide to become industrially viable in lithium-ion batteries, we believe that the reversibility of Li_2O formation must be optimized while maintaining inexpensive production costs.

In this study, we report a novel method of synthesizing a tin oxide carbon composite (SnO_x-C) through the solid-state pyrolysis of a single complexed tin and carbon precursor. This synthesis resulted in the formation of tin oxide nanoparticles embedded in a flexible, porous carbon support. To the best of the authors' knowledge, the only previous study that employed a complexed precursor to form a tin oxide-carbon composite did not fully explore the mechanisms for its excellent cycling stability.[34] In our study, we not only used a simpler synthetic method but also elucidated the mechanism for the electrochemical performance improvement, compared to noncomposite tin oxide electrodes.

Electrochemical cycling of the SnO_x-C composite displays its properties as a robust, high capacity anodic material for lithium-ion batteries. The SnO_x-C composite exhibited (i) an initial capacity of 542 mAh g^{-1} with 80.6% capacity retention over 400 cycles at a high current density of 900 mA g^{-1} (1C), (ii) an initial capacity of 667 mAh g^{-1} with 88.7% capacity retention at a lower current density of 450 mA g^{-1} (C/2) over 400 cycles, and (iii) an initial capacity of 710 mAh g^{-1} with 88.8% capacity retention at a current density of 180 mA g^{-1} (C/5) over 400 cycles. To determine the reason for this excellent performance, we analyzed the structure and composition of the SnO_x-C using X-ray diffraction (XRD), X-ray photoelectron spectroscopy (XPS), electrochemical analysis, and time-of-flight secondary ion mass spectrometry (TOF-SIMS) depth profiling analysis. The results of which suggest the unique architecture of the SnO_x-C, which promotes reversibility of Li_2O, prevents tin aggregation, and suppresses volume expansion, thereby preventing particle fracture. Scheme 1 illustrates how SnO_x-C counteracts the detrimental effects of tin oxide lithiation.

EXPERIMENTAL METHODS

Materials. All chemicals were used as received, unless otherwise noted. The following chemicals were used in the synthesis of the SnO_x-C active material. Tin chloride anhydrous ($SnCl_2$) and sucrose ($C_{12}H_{22}O_{11}$, 99.0%) were purchased from Alfa Aesar. Sodium hydroxide (NaOH, 98.8%) was purchased from Fisher Chemical. Citric acid monohydrate [$(HOC(COOH)(CH_2COOH)_2 \cdot H_2O$, 99.0%] was purchased from Sigma-Aldrich. The following chemicals were used for the fabrication of SnO_x-C lithium ion batteries. Super P was used as a conductive additive and was purchased from MTI Corporation. Carboxy methyl cellulose was used as the binder for the active materials and was purchased from Sigma-Aldrich. Lithium hexafluorophosphate ($LiPF_6$; 99.99%) and diethyl carbonate (DEC; 99%) were purchased from Sigma-Aldrich, and fluoroethlyene carbonate (FEC, +99%) was acquired from Solvay. Li foil was purchased from Alfa Aesar. Celgard 2400 microporous monolayer membranes (polypropylene, 25 μm) were obtained from Celgard.

Synthesis of the Ditin Citrate Precursor. Procedures were derived and scaled up from Deacon et al.[35] Citric acid monohydrate (7.13 g, 33.9 mmol) was introduced into deoxygenated water (135 mL) and allowed to stir until fully dissolved, after which $SnCl_2$ anhydrous (15.0 g, 79.1 mmol) was added to the solution. This mixture was stirred for 20 min to ensure full dissolution of $SnCl_2$. During this time, a 2 M NaOH solution was made using deoxygenated water (67.5 mL). After sufficient stirring, the NaOH solution was introduced into the reaction mixture dropwise over a period of 30 min. A white precipitate formed as the solution rose above a pH of 5.0. Care was taken to not let the solution pH rise above 12, as this would have induced the formation of tin hydroxide. The reaction was conducted with constant sparging of N_2 to eliminate any undesired side-reactions. The resulting precipitate was filtered off and then rinsed three times with water and ethanol, respectively. The product was then dried under vacuum overnight at 70 °C. The resulting product was a fine, white powder. Yield: 13.6 g (94.4%). ^{13}C

DOI: 10.1021/acsaem.9b01205
ACS Appl. Energy Mater. 2019, 2, 7244−7255

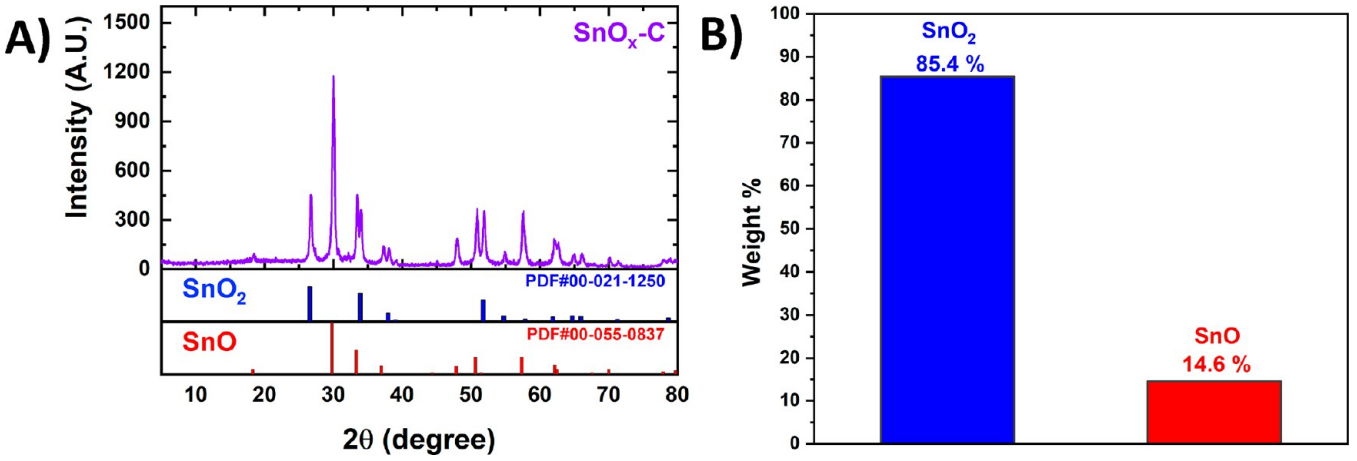

Figure 1. (A) X-ray diffraction pattern of the SnO_x-C composite. Literature diffraction patterns of SnO_2 (PDF #00-021-1250) and SnO (PDF #00-055-0837) have been included for reference. (B) Composition of the tin oxide species contained within the SnO_x-C Composite. Concentration of each species was determined through whole pattern X-ray diffraction fitting using the respective literature diffraction patterns.

CP MAS NMR data: δ 50.0 (CH2), 54.7 (CH2), 81.2 (tertiary C), 180.2 (CH_2CO_2Sn), and 183.4 (R_2CO_2Sn).

Synthesis of the SnO_x-C Composite. Ditin citrate and sucrose were mechanically combined using a mortar and pestle in a 1:1 weight ratio. The resulting mixture was then placed in a ceramic crucible and pyrolyzed using a horizontal tube furnace (MTI, OTF-1200X) under argon atmosphere. The mixture was heated to 550 °C at a rate of 10 °C/min, followed by a 2 h heat soak at 550 °C to ensure homogeneous polymerization throughout the material. The product was then cooled to room temperature. The resulting product (SnO_x-C) was mechanically homogenized using a mortar and then collected.

Fabrication of SnO_x-C Electrodes. Slurries of the SnO_x-C composite material were fabricated using active material, Super P, and sodium-carboxymethyl cellulose (Na-CMC) in an 85:10:5 mass ratio dispersed in water. Na-CMC was chosen for its exceptional performance with materials that undergo large volumetric expansion during galvanostatic cycling.[36] The resulting slurry was cast onto cleaned copper foil with a doctor blade (MTI, AFA-I). The slurry-coated film was immediately placed in an oven to dry at 120 °C for 5 h. After initial drying, the film was placed under vacuum at 120 °C to dry overnight. Circular electrodes (7/16 in. diameter) were cut from the slurry cast film and placed under vacuum overnight before use to ensure residual water was driven off.

Electrochemical Characterization of SnO_x-C Electrodes. Four-point probe measurements of the pristine SnO_x-C material thickly coated on a glass substrate were conducted utilizing a manual four-point resistivity probe (Lucas S302; Lucas Laboratories). Sheet resistivity was determined by measuring the potential at various applied currents. The sheet resistivity was then calculated via a modified version of Ohm's law. Calculations, methodology, and results are further described in the SI. Cycling performance and cyclic voltammetry (CV) tests were conducted using a multichannel battery test system (BT 2043, Arbin). Anode materials were assembled in 2032 stainless steel coin cells versus Li foil (Alfa Aesar) as the counterelectrode. Celgard 2400 membranes (25 μm, Celgard) were used as the cell separator. The electrolyte was composed of 1 M lithium hexfluorophosphate ($LiPF_6$) in fluoroethylene carbonate (FEC)/diethyl carbonate (DEC) (1:1 by volume) solution. Excess electrolyte was used (>5 drops) to flood the cell and to provide sufficient wetting. All galvanostatic cycling was conducted with a potential window of 5 mV to 3.0 V. This potential window was chosen to establish stability at high voltages and to replicate standard anode half-cell performance testing practices found in the literature.[1,15,37−39] Three conditioning C/20 cycles were run for all tested cells to form a consistent SEI prior to commencing galvanostatic charge/discharge tests. An example of a typical conditioning procedure is demonstrated in Figure S7 All presented electrochemical plots are averages of two identical cells to provide reproducibility of our results. Active mass loadings of the SnO_x-C electrodes were kept within a range of 2.5−3.4 mg/cm^2. Rate capability testing was conducted where the cells were run at a C/20 for 3 cycles, C/10 for 5 cycles, C/5 for 5 cycles, C/4 for 5 cycles, C/2 for 5 cycles, 1C for 5 cycles, 2C for 5 cycles, and finally the system was recovered at C/10 to examine the capacity retention. For long-term stability tests, all cells underwent three C/20 formation cycles followed by long-term cycling at the detailed cycling rate/current density. Full cell cycling of the SnO_x-C material was conducted by employing a NCM (6-2-2) cathode as the counterelectrode. Slurries of NCM (6-2-2) were cast onto aluminum foil and demonstrated a mass loading of 6.5−7.5 mg/cm^2. Half-cell electrochemical performance of the NCM cathode can be found in the electrochemical analysis section of the SI. Full cell configurations were generated using an N/P ratio of 1.2:1, in order to prevent the plating of lithium metal. Prelithiation was conducted on the anode material to prevent loss of lithium through the first low Coulombic efficiency cycle.

Material Characterization. X-ray diffraction patterns were obtained with a Rigaku Miniflex 600 diffractometer utilizing Cu Kα radiation (λ = 1.5418 Å). Diffraction patterns were analyzed from 5−80° in a continuous scan mode (2° min^{-1}) with a step width of 2θ = 0.025°. Thermographs of the precursor materials and the composite's thermal stability were taken using a Mettler Toledo thermogravimetry (TGA)/differential scanning calorimetry (DSC) 1 STAR^e system. Decomposition profiles were generated under nitrogen atmosphere using a temperature window of 30−750 °C and a heat ramp of 10 °C/min. Sample mass ranged from 7 to 10 mg. A Witec Micro-Raman spectrometer, equipped with a 40 W blue laser, was used to acquire the Raman shift of the composite. An excitation wavelength of 488 nm and a spectral center of 2498 cm^{-1} were employed to acquire the Raman shift invoked by the graphitized carbon. XPS spectra were recorded using a monochromated 120 W Al−Kα1 X-ray source ($h\nu$ = 1486.5 eV), hybrid optics (employing a magnetic and electrostatic lens simultaneously) and a multichannel plate coupled to a hemispherical photoelectron kinetic analyzer. Time-of-flight secondary−ion mass spectrometry (TOF−SIMS) was conducted using an ION-TOF GmbH (2010) instrument. TOF−SIMs analysis was employed to characterize the reversibility of tin oxide (de)lithiation. Further details on the experimental procedures used for each analytical technique can be found in the SI of this manuscript.

RESULTS AND DISCUSSION

Synthesis of the SnO_x-C Composite. Synthesis of the precursor, ditin citrate, was conducted through a simple anion exchange precipitation reaction between tin chloride and citric acid. The result of this synthesis was a dense, white powder. Because of its insoluble characteristic and a lack of previous

DOI: 10.1021/acsaem.9b01205
ACS Appl. Energy Mater. 2019, 2, 7244−7255

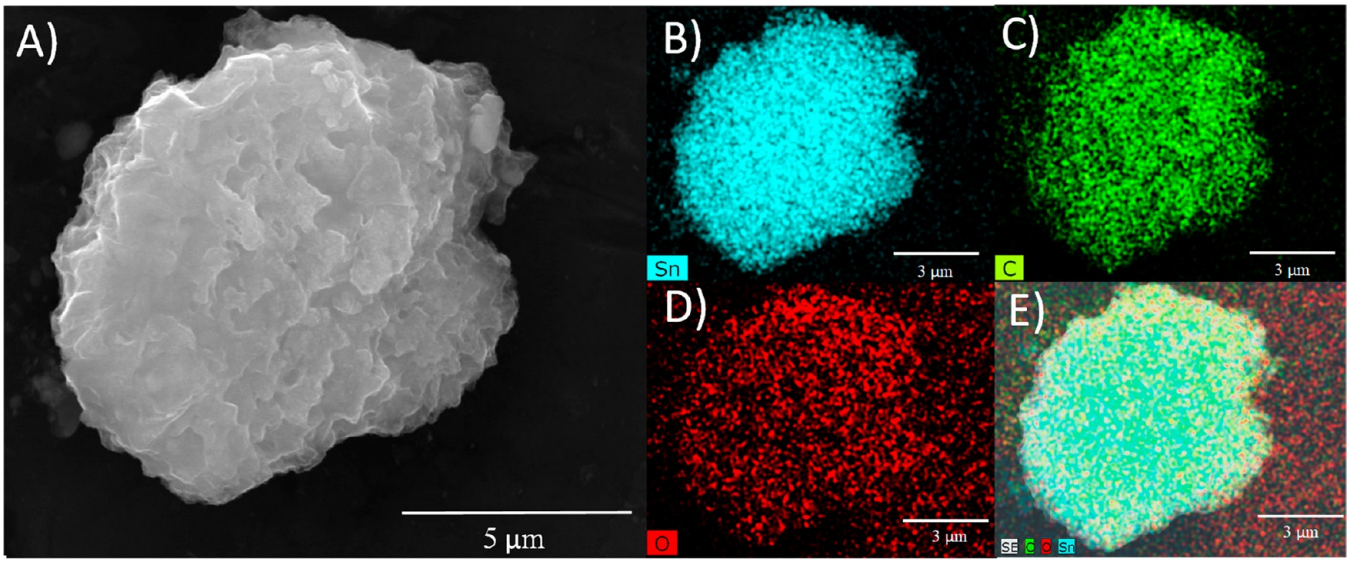

Figure 2. (A) SEM micrograph of the SnO_x-C composite. (B–E) EDX elemental mapping of tin, carbon, oxygen, and region mapping; respectively.

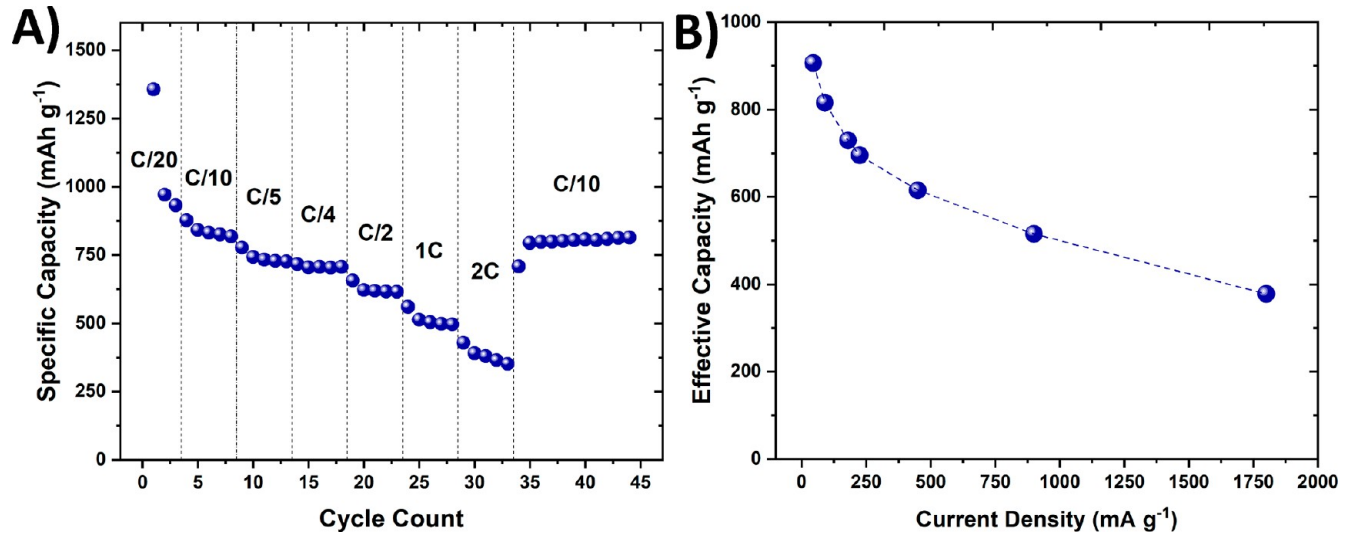

Figure 3. (A) Variable rate galvanostatic cycling of SnO_x-C versus Li. (B) Effective gravimetric capacity of SnO_x-C composite at various current densities.

characterization, qualitative purity analysis was conducted through solid state C^{13}-NMR as seen in Figure S1. The results of this analysis clearly depict the formation of ditin citrate. For results of the aforementioned analysis and schemes of the reaction, see the SI.

Formation of the tin oxide-carbon composite was conducted through the use of pyrolysis reactions in inert atmospheres. We were interested in exploring tin oxide because of its high gravimetric capacity and the need to extend the cycle life of this material. Our goal was to pyrolyze to graphitic carbon, which is more efficiently formed at high temperatures (exceeding 600 °C); however, tin oxide is known to reduce to metallic tin in the presence of carbon at temperatures above 600 °C in inert atmospheres. For these reasons, synthetic temperatures were kept to 550 °C.[40] Thermal gravimetric analysis of ditin citrate reveals that only approximately 5% of the carbon remains after pyrolysis (Figure S2A). Because of the large volumetric expansion of tin oxide during lithiation (~300%), supplemental carbon is required to prevent fracturing of the particles.[7,9,13] Sucrose was employed as the carbon additive due to its low graphitization temperature and tendency to form porous, flexible carbon.[41] Compared to nanomaterials, micron-sized materials tend to have higher tap densities and are cheaper to manufacture. To maintain practicality, synthetic conditions were tuned for the creation of micron-sized particles. Maintaining the pyrolysis temperatures at 550 °C also prevented thermal reduction of the tin oxide.[40,42] The X-ray diffraction (XRD) pattern, as seen in Figure 1A, confirms that the product of the pyrolysis of ditin citrate/sucrose (1:1) was indeed SnO_x-C, and the sharp, defined peaks of the pattern indicate that the product was composed of tin(IV) oxide and tin(II) oxide. Furthermore, a whole pattern fitting technique was applied to the diffraction pattern of SnO_x-C, revealing that approximately 85 wt % of the tin oxide consists of SnO_2, whereas approximately 15 wt % consist of SnO. Full parameters and procedures of this quantification are detailed the SI. There are no sharp, defined peaks for the carbon constituent of the composite. Thermal

DOI: 10.1021/acsaem.9b01205
ACS Appl. Energy Mater. 2019, 2, 7244–7255

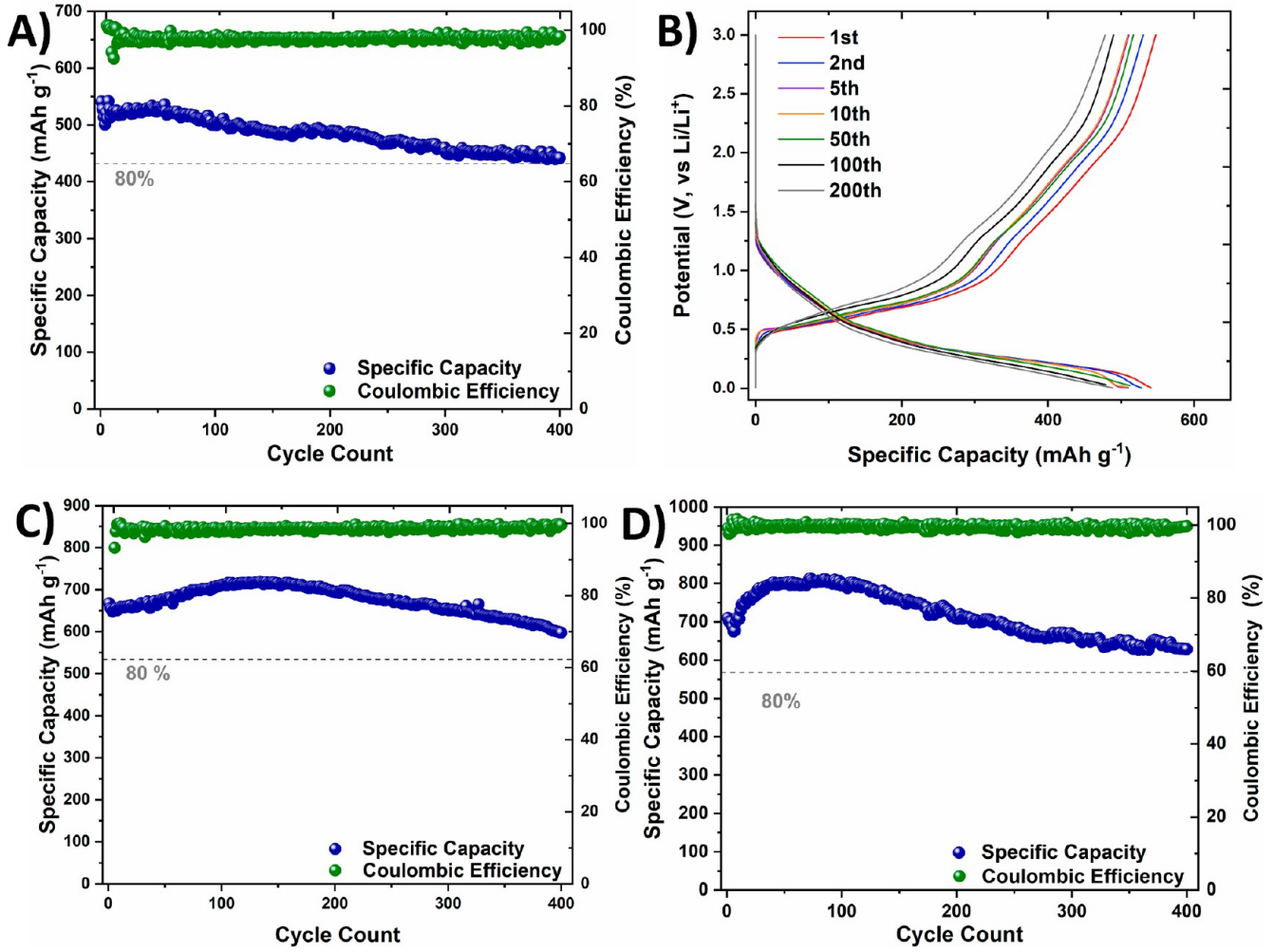

Figure 4. Long-term electrochemical analysis of the SnO_x-C composite versus Li. (A) Cycling performance at 900 mA g^{-1} (1C) current density. (B) Charge−discharge profile at 900 mA g^{-1} (1C). (C) Cycling performance at 450 mA g^{-1} (C/2) current density. (D) Cycling performance at 180 mA g^{-1} (C/5) current density.

gravimetric analysis (TGA) of the composite material was conducted in ambient atmosphere to burn away the carbon framework and in turn determine the total carbon content. Results of this analysis, Figure S3, suggest that approximately 28 wt % of the composite consists of carbon, whereas 72 wt % of the composite consists of tin oxide.

Scanning electron microscopy/energy-dispersive X-ray spectroscopy (SEM/EDX) micrographs of the SnO_x-C composite were taken to determine the resulting chemistry and morphology (Figure 2). Imaging of the composite material suggests that the particles are coated in a layer of porous carbon that completely surrounds the interior tin oxide particles. To affirm this qualitative assessment, a surface sensitive technique, XPS, was used to analyze the exterior of this composite material. High-resolution XPS spectra were taken of the material for the C 1s, O 1s, and Sn 3d regions. Because of the 5−15 nm penetration depth of this technique, we were able to determine the consistency of the carbon coating. Quantitative analysis of the XPS spectra (Figure S4E) shows that the composite material is uniformly coated, exhibiting only 0.59 atom. % of exposed tin on the surface compared to carbon. Deconvolution of the high-resolution spectra was used to determine the functionality of the surface carbon as seen in Figure S4B−D. The study also revealed that the carbon framework contained various oxygen functionalities. The role of the oxygen-functionalized carbon is discussed at length later in the manuscript.

Electrochemical Analysis of the SnO_x-C Composite. The electrochemical properties of the SnO_x-C composite were obtained via variable rate cycling with rates ranging from C/20 to 2C (Figure 3). The results demonstrate that the material is capable of high capacity lithiation at both low (C/20) and high (2C) current densities. Furthermore, the capacity recovery after returning to C/10 cycling affirms the robustness of the material, suggesting that its structure is not damaged by high current density cycling. Lifetime cycling analysis of the material was conducted at current densities of 1C, C/2, and C/5 (Figure 4). Industry standards suggest that the lifetime of a material is based on how long the material can retain 80% of its highest initial capacity. As such, all figures have included a dashed line to denote the effective cycle life of the material under the various long-term cycling parameters. It can be noted that the galvanostatic cycling shown in Figures 3 and 4 demonstrates consistent results for their effective initial capacities. Long-term electrochemical cycling demonstrates that the SnO_x-C composite exhibits a reversible capacity of 900 mA g^{-1} after 400 cycles (80.6% retention) with a current density of 900 mA g^{-1} (1C). Alternatively, the material has a

DOI: 10.1021/acsaem.9b01205
ACS Appl. Energy Mater. 2019, 2, 7244−7255

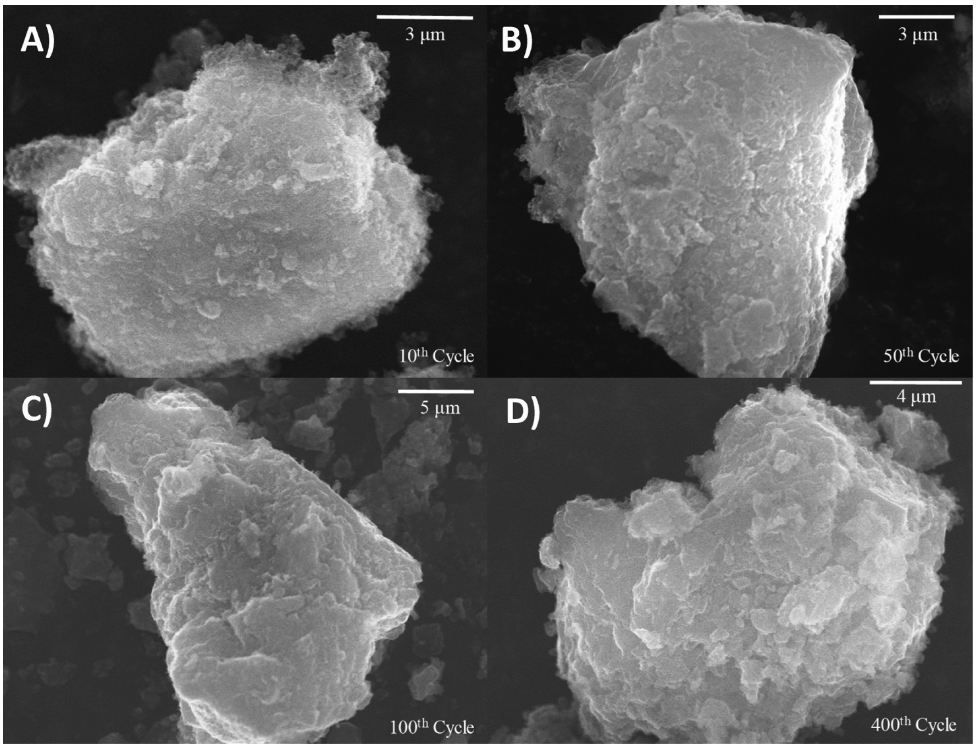

Figure 5. (A–D) Post-mortem scanning electron micrographs of the SnO_x-C particles after 10, 50, 100, and 400 cycles, respectively.

lithiation capacity of 592 mAh g^{-1} after 400 cycles (88.7% retention) at 450 mA g^{-1} (C/2) and 629 mAh g^{-1} after 400 cycles (88.8% retention) at a current density of 180 mA g^{-1} (C/5). To obtain a better understanding of the principles behind the enhanced cycling performance, various analyses were conducted to examine the inherent architecture and potential mechanisms involved in the lithiation of SnO_x-C.

Investigation of SnO_x-C Architecture. The high-resolution SEM imaging suggests the carbon coating to be porous in composition, leading to better diffusion of lithium-ions into the interior. SEM/EDX imaging provides interesting details about the structural morphology but only provides a qualitative assessment for the overall architecture of the composite. Brunauer–Emmett–Teller (BET) analysis was performed on the composite to obtain a quantitative assessment of the pore architecture. N_2 adsorption isotherms (at 77 K) were collected to evaluate the specific surface area and pore characteristics of the SnO_x-C (Figure S13). The measured surface area, 210 m^2 g^{-1}, suggests the generation of a porous material (Table S2). Furthermore, quenched-solid density functional theory (QSDFT) analysis reveals the hierarchically porous character of the material, having an average pore size of 1.03 nm (Figure S14). The permeable architecture of the composite is essential to the Li^+ storage potential for the micron-size material. Micron-sized composite particles could impede the penetration of Li^+, thereby preventing total accessibility of lithium storage sites.[43] The existence of this pore structure likely endows this composite material with superior electrochemical performance by allowing the electrolyte to wet both the supporting carbon matrix and the tin-oxide nanocrystals, consequently enhancing the lithium ion transport throughout the structure during cycling. These elucidated textural properties support the high Coulombic efficiency and stability of this material at fast charging rates.

The carbon support surrounding the tin oxide nanoparticles acts as a volumetric expansion buffer during lithiation and a means of enhancing the electrical conductivity of the overall material. Fully graphitized carbon is often brittle and is a poor expansion buffer for the composite. On the other hand, disordered graphite is known to have enhanced flexibility and mechanical strength.[44] To determine the degree of graphitization within the material, Raman spectroscopy was employed to examine the D and G bands of the carbon. An I_D/I_G ratio is commonly used to determine the degree of graphitization for carbonaceous species.[45−47] Figure S5 depicts the deconvolution of these bands and reveals the semigraphitized nature of the carbon through an I_D/I_G ratio of 0.76. The semigraphitized nature of the carbon suggests how the composite material is able to retain effective capacity even after 400 cycles of large expansion lithiation. Furthermore, four-point probe analysis (Table S1) demonstrates that this carbon shell has heightened the electrical conductivity of the composite (σ = 19.6 ± 0.4 S/m), increasing the material's viability as an anodic material in advanced lithium ion batteries.

Both the long cycle life and the considerable disorder of the carbon coating lead us to believe that this material is resistive to cracking caused by large volumetric expansion during lithiation. To verify this, post-mortem SEM imaging of the SnO_x-C material was conducted after 10, 50, 100, and 400 cycles of 180 mA g^{-1} current density galvanostatic cycling, Figure 5. Scanning electron micrographs of the material suggest that the composite particles retained structural integrity throughout the 400 cycles. There is a slight degradation to the exterior, typical of long-term, high-density galvanostatic cycling, yet no visible fractures or cracks in the particles were seen in the high-magnification analysis. This suggests that the carbon coating is in fact buffering the volumetric expansion of the tin oxide particles.

DOI: 10.1021/acsaem.9b01205
ACS Appl. Energy Mater. 2019, 2, 7244−7255

Investigation of the SnO_x-C Lithiation Mechanism. The analysis of the inherent architecture has revealed some of the fundamental components for electrochemical performance enhancement. To better elucidate the cycling mechanisms of the SnO_x-C composite, cyclic voltammetry was employed to examine the reversible, electrochemical processes occurring during lithiation and delithiation of the composite material (Figure 6). Long-term voltammograms reveal that the material

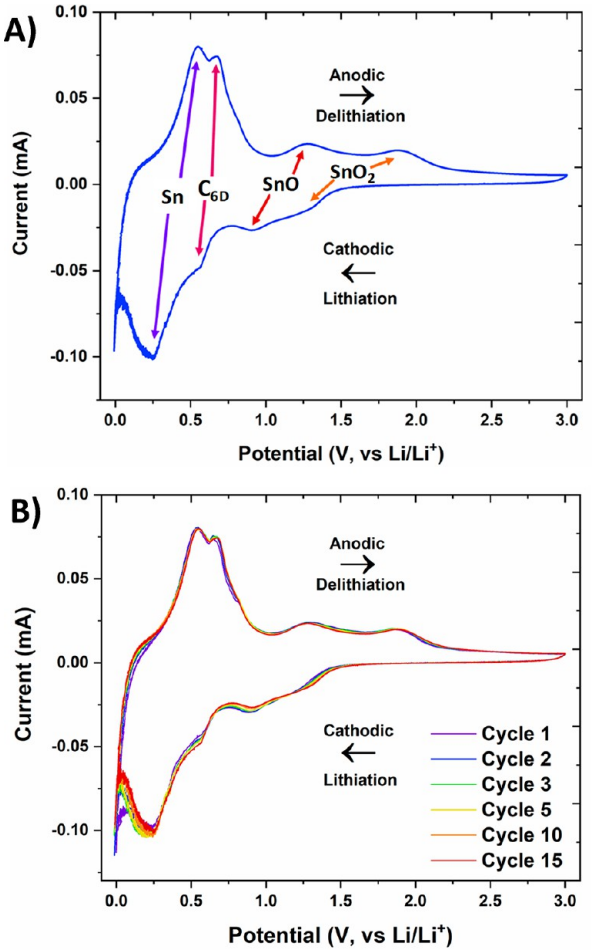

Figure 6. Cyclic voltammograms of SnO_x-C versus Li with a potential window of 5 mV to 3.0 V and generated from a 0.1 mV/s scan rate. (A) Cyclic voltammogram of the first cycle with lithiation/delithiation potentials denoted. (B) Long-term cyclic voltammograms from 1 to 15 cycles.

undergoes fully reversible lithiation with minimal change in the extent of the electrochemical lithiation/delithiation. As indicated by the peaks on either side of ∼1.1 V and ∼1.5 V on both the anodic and cathodic scans, the material depicts reversible lithiation of SnO and SnO_2, respectively. Many tin oxide anode materials are unable to employ the reversible formation of Li_2O during cycling.[14−19] Experimental[11,31,32,48] and theoretical studies[9,10] on the formation of Li_2O have shown that reversible delithiation can only effectively be achieved with tin oxide nanoparticles and if the Li_2O matrix remains unperturbed during cycling. Cross-sectional analysis of the SnO_x-C composite, shown in Figure 7, provides insight as to how the micron-sized SnO_x-C composite is able to obtain reversible formation of Li_2O. Cross-sectional SEM imaging reveals that the composite consists of tin oxide nanoparticles embedded within a carbonaceous framework. The formation of the nanoparticles is attributed to the use of a tin and carbon containing precursor. It is hypothesized that the carbon support acts as a barrier in situ, preventing the clustering of tin oxide particles during synthesis. The novel precursor allows for facile synthesis of a high-tap density, micron-sized composite particles that reap the benefits of the nanosized particles of tin oxide, such as improved ionic conductivity and reversibility of Li_2O formation.[9−11,31,32,48−50]

The newly formed Li_2O matrix must remain undisturbed during cycling. Disruptions in the matrix can lead to less interactions between the Li_2O and metallic tin, thereby reducing the reversibility of the Li_2O formation.[9,10] These perturbations can occur from both the aggregation of tin atoms during cycling and the large volumetric expansion. The architecture of the SnO_x-C composite can lead to retention of the matrices during cycling based on two methodologies. (1) The first being that the regions containing the tin oxide nanoparticles are closely interlocked and held in place by semigraphitized carbon. The semigraphitized carbon framework not only acts as an expansion buffer during lithiation but also acts as a barrier, preventing dispersion of the Li_2O matrix and aggregation of tin atoms during delithiation. This is supported by the cross-sectional analysis of SnO_x-C (Figure 7) showing the tin oxide nanoparticles entrapped within a framework of carbon. (2) Furthermore, oxygen functionalities of the carbon employ ionic interactions to prevent the dispersal of the Li_2O during cycling. Sucrose is a graphite precursor known for its production of low-temperature, oxygen-functionalized carbon. XPS analysis of the composite material (Figure S4) details the ample oxygen functionalities of the carbon support. Oxygen-functionalized carbon is used in lithium−sulfur batteries to prevent the dissolution of lithium sulfide intermediates during cycling.[51−53] The oxygen functional groups provide anionic interactions which trap the intermediates in place and prevent their dissolution.[51−53] We hypothesize that these functional groups operate in a similar manner to those in lithium−sulfur batteries, acting as a means of ionic interactions that seem to lock the Li_2O in place during cycling.

Electrochemical, optical, and spectroscopic data suggest that the carbon framework of the composite helps to supplement the performance of the tin oxide by acting as an expansion buffer, preventing clustering of tin, and aiding in the retention of the Li_2O matrix while cycling. To affirm these results an investigation of the interior morphology after cycling was conducted in a similar manner to the cross sections shown in Figure 7. Post-mortem cross-sectional SEM/EDX imaging of the SnO_x-C composite was obtained by embedding the electrode material (from Figure 5D) after 400 galvanostatic cycles in silver epoxy. The resulting micrographs are found in Figure 8. The images establish that the interior morphology is virtually identical to that depicted by the cross-sectional imaging of the pristine SnO_x-C particles. Furthermore, no interstitial cracks were found in the composite, even after 400 cycles. This suggests that the loss in capacity can be attributed to slow degradation of the exterior upon high current density cycling and the carbon reacting with the electrolyte.

The reversible formation of Li_2O is a contentious subject in the field of tin oxide anodes as many electrodes are not able to achieve any reversibility at all. However, theoretical[9,10] and experimental[11,31−33,48] studies employing tin oxide nanoparticles have shown reversible formation is possible. To

DOI: 10.1021/acsaem.9b01205
ACS Appl. Energy Mater. 2019, 2, 7244−7255

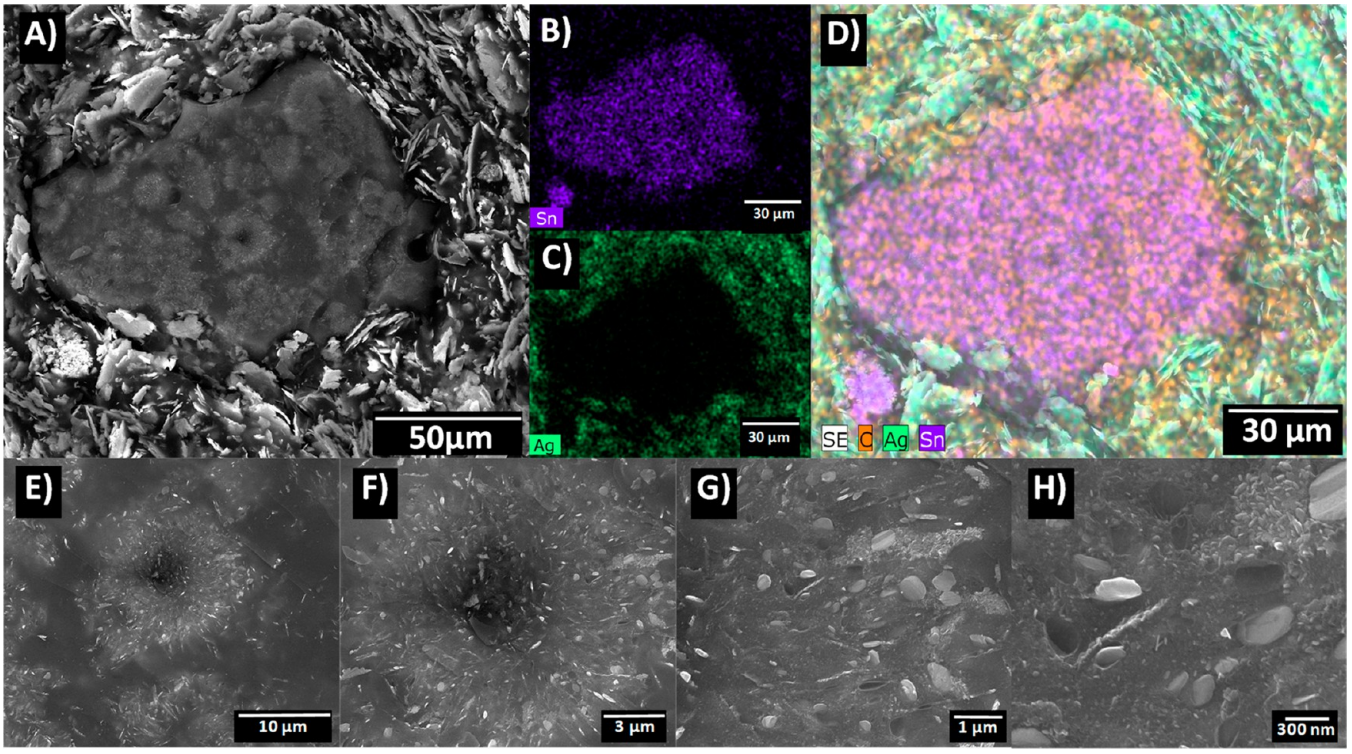

Figure 7. Cross-sectional analysis of microtomed SnO_x-C particle embedded in silver epoxy. (A) SEM micrograph of SnO_x-C particle in epoxy. (B–D) EDX elemental mapping of tin, silver, and region mapping, respectively; highlighting the SnO_x-C particle. (E–H) High-resolution SEM micrographs displaying the presence of tin oxide nanoparticles embedded in the carbon framework.

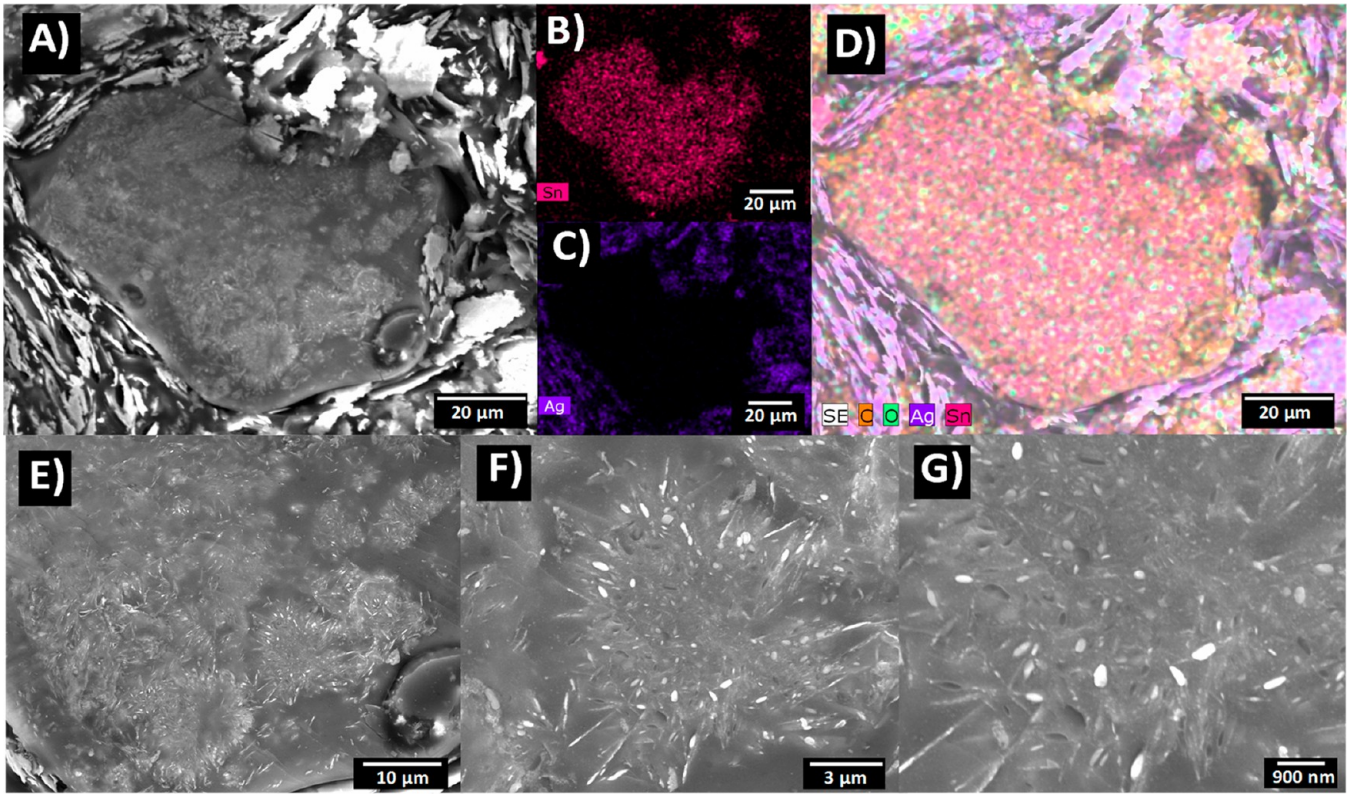

Figure 8. Cross-sectional micrograph of the SnO_x-C composite particle embedded in a silver epoxy after 400 cycles of galvanostatic charge and discharge at a current density of 170 mA/g. (A) SEM micrograph of SnO_x-C particle in epoxy. (B–D) EDX elemental mapping of tin, silver, and region mapping, respectively, highlighting the SnO_x-C nanoparticles. (E–G) High-resolution SEM micrographs display the presence of tin oxide nanoparticles embedded in the carbon framework.

DOI: 10.1021/acsaem.9b01205
ACS Appl. Energy Mater. 2019, 2, 7244–7255

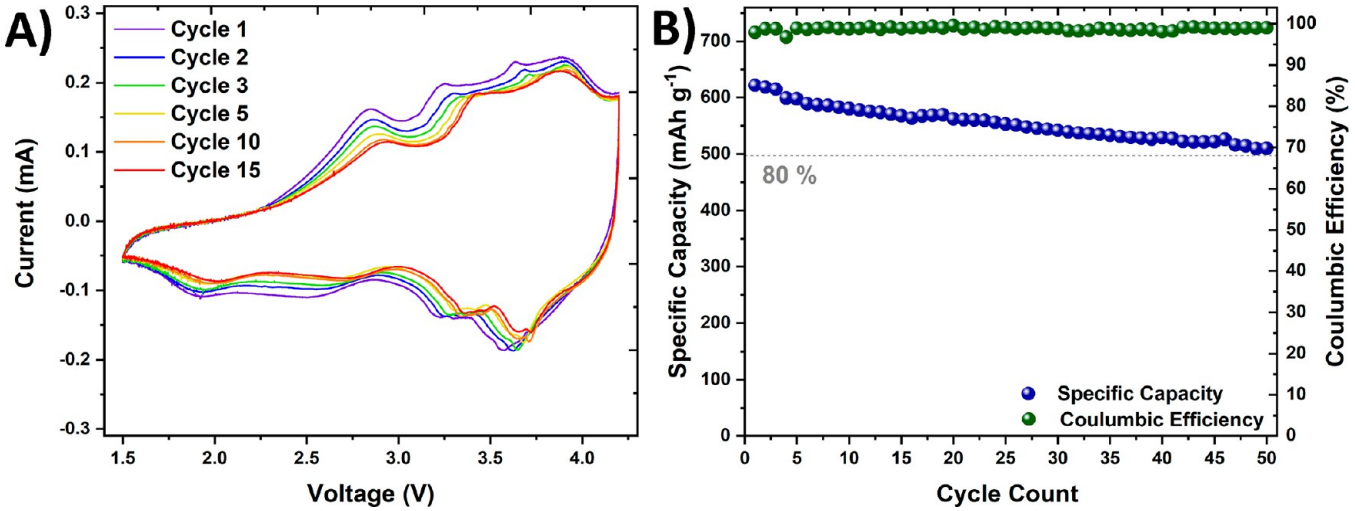

Figure 9. Electrochemical analysis of the SnO_x-C versus NCM full-cell system. (A) Long-term cyclic voltammograms generated with a potential window of 1.5−4.2 V and 0.1 mV/s scan rate. (B) Galvanostatic cycling performance at C/2 (450 mA g^{-1} for anode, 90 mA g^{-1} for cathode) cycling rate.

further confirm our CV results demonstrating reversible formation of Li_2O, we conducted an innovative post-mortem TOF-SIMS analysis of the electrodes after one discharge and one full cycle, respectively. The resulting TOF-SIMs analysis can be found in Figure S6. Because the analysis is performed between two initially identical materials, quantification of the LiO^- ion can be performed to determine the amount of reversible Li_2O formed within the first cycle. To ensure consistency throughout the samples, all LiO^- curves were normalized to the respective Sn^- content of each sample. Quantification of this ion suggests that approximately 50% of the Li_2O is reversible within the first cycle. This result affirms the conclusions reached through our cyclic voltammograms. Previously, many publications have stated the irreversibility of Li_2O formation, therefore finding reversibility to this extent elucidates the interesting electrochemical properties of the ditin citrate dervied material. The initial Coulombic efficiencies of conversion materials are usually relatively low, often near 50%. This result explains why the initial Coulombic efficiency of our material is 69.94% (Figure S6). This high initial Coulombic efficiency suggests the SnO_x-C material would act as a viable candidate in electrochemical full cell systems.

To test the viability of the SnO_x-C composite as a candidate for practical lithium-ion batteries, full-cell electrochemical analysis of SnO_x-C versus NCM (622) was conducted. One of the main concerns with utilizing a tin oxide anode in full-cell applications is the high lithiation potential. Because of NCM's high operating voltage, NCM was chosen as the counter-electrode so that the electrochemical cell could supply satisfactory power. Figure 9A displays long-term cyclic voltammograms of the full-cell SnO_x-C system and supports the reversibility of Li_2O formation within the SnO_x-C composite. To mimic the desired properties of commercial batteries, long-term galvanostatic cycling (Figure 9B) was conducted at fast-cycling rates with an N/P ratio of 1.2:1. Results of this galvanostatic cycling show that the SnO_x-C composite is able to demonstrate an initial lithiation capacity of 621 mAh g^{-1} and an 82.3% capacity retention after 50 cycles while applying a C/2 charge/discharge rate.

In summary, implementation of a complexed precursor has led to the production of tin oxide nanoparticles embedded in a flexible carbon framework through simple solid-state pyrolysis. We hypothesize that the carbon support acted as a barrier preventing the aggregation of tin oxide during synthesis thereby allowing us to easily form tin oxide nanoparticles. The disordered, porous nature of the semigraphitized carbon allows this support to act as a barrier against tin aggregation and volumetric expansion during lithiation. These characteristics allowed SnO_x-C to display a lithiation potential of 667 mAh g^{-1} with nearly 89% capacity retention after 400 cycles of 450 mA g^{-1} current density cycling. CV and TOF-SIMs analysis suggest this superior capacity retention can also be attributed to the enhanced reversibility of Li_2O formation. Furthermore, we hypothesize that the oxygen-functionalized carbon forms ionic interaction with the Li_2O thereby leading to better retention of the Li_2O matrix during cycling and in turn increasing the reversibility of Li_2O formation. We believe the architecture and methodology used in this composite can be used in future materials to invoke enhanced electrochemical performance.

CONCLUSIONS

In this study, we reported the synthesis of a SnO_x-C composite through the use of a novel precursor, ditin citrate. Simple solid-state pyrolysis of the complexed precursor resulted in the production of a composite containing tin oxide nanoparticles embedded in a flexible carbon support. Through a systematic analysis of the architecture, using high-resolution X-ray photoelectron spectroscopy, Raman spectroscopy, cross-sectional and post-mortem scanning electron microscopy, and Brunauer−Emmett−Teller (BET) analysis, we examined how the resulting structure aided in the reversible lithiation/delithiation of the tin oxide material. The presence of tin oxide nanocrystals provides a more thermodynamically favorable environment for Li_2O reversibility and enhances ionic conductivity. The semigraphitized carbon framework acts as a volumetric expansion buffer, aids in preventing aggregation of tin oxide particles during lithiation, and enhances the electrical conductivity of the composite. The presence of the oxygen functional groups on the carbon support is hypothesized to aid in the retention of the Li_2O matrix during cycling, thereby enhancing the reversibility of the Li_2O formation.

DOI: 10.1021/acsaem.9b01205
ACS Appl. Energy Mater. 2019, 2, 7244−7255

Electrochemical analysis of the SnO_x-C composite reveals its exceptional electrochemical potential as an anode material for lithium-ion batteries. Cyclic voltammetry demonstrates the high reversibility of the alloying and conversion reactions of SnO_x-C lithiation. Long-term galvanostatic testing of the composite material exhibits the material's potential for high gravimetric capacities, high Coulombic efficiencies, and extended cycle life. The proficient electrochemical properties have been attributed to the presence of tin oxide nanocrystals; a flexible, oxygen-functionalized carbon framework, and the reversible formation of Li_2O throughout cycling. We believe that this study presents a material with improved capacity retention, whereas the systematic analysis of the architecture also acts as a fundamental study that could provide other researchers with insights on how to improve the cyclability of other metal oxide-carbon composites through the utilization of similar architectures and synthetic methods. Considering the performance and simplicity of this composite, this synthetic strategy may provide new insight into the design of other electrochemical materials with promising lithium-storage properties. Other works have shown satisfactory performance of tin oxide anodes in sodium- and potassium-ion batteries, therefore future work will examine how this architecture or similar motifs can further enhance the reversibility of tin oxide in other alkali ion batteries.[30,54,55]

■ ASSOCIATED CONTENT

Supporting Information

The Supporting Information is available free of charge on the ACS Publications website at DOI: 10.1021/acsaem.9b01205.

Detailed procedure of the synthesis of the ditin citrate precursor and SnO_x-C composite; thermal gravimetric analysis of sucrose and ditin citrate precursors; four-point probe electrical conductivity measurements of the SnO_x-C composite; high-resolution X-ray photoelectron spectroscopy analysis of SnO_x-C surface; Raman spectroscopy of SnO_x-C; cross-sectional analysis of the post-mortem SnO_x-C composite embedded in silver epoxy; time-of-flight simulated imaging mass-spectrometry examining the quantification of reversible tin oxide (de)lithiation; galvanostatic data of SEI formation cycles; electrochemical analysis of NCM cathode; electrochemical analysis of comparative tin oxide materials; Brunauer–Emmett–Teller and quenched-solid density functional theory analysis of SnO_x-C composite; and quantification of the tin oxide species. (PDF)

■ AUTHOR INFORMATION

Corresponding Author

*E-mail: mullins@che.utexas.edu.

ORCID

Andrei Dolocan: 0000-0001-5653-0439

Adam Heller: 0000-0003-0181-1246

C. Buddie Mullins: 0000-0003-1030-4801

Author Contributions

The manuscript was written through contributions of all authors. All authors have given approval to the final version of the manuscript.

Notes

The authors declare no competing financial interest.

■ ACKNOWLEDGMENTS

The authors gratefully acknowledge the Welch Foundation for support of this work (Grants F-1131 (AH) and F-1436 (CBM)) as well as the National Science Foundation via Grant CBET-1603491. The authors would like to thank the National Science Foundation's Major Research Instrumentation Program for providing us with the instrumentation to conduct solid-state NMR via Grant CHE-1626211. The authors also thank Celgard for generously supplying membrane separators and Solvay for providing fluoroethylene carbonate.

■ REFERENCES

(1) Schipper, F.; Aurbach, D. A Brief Review: Past, Present and Future of Lithium Ion Batteries. *Russ. J. Electrochem.* **2016**, *52* (12), 1095–1121.

(2) Zubi, G.; Dufo-López, R.; Carvalho, M.; Pasaoglu, G. The Lithium-Ion Battery: State of the Art and Future Perspectives. *Renewable Sustainable Energy Rev.* **2018**, *89*, 292–308.

(3) Li, Y.; Lu, Y.; Adelhelm, P.; Titirici, M.-M.; Hu, Y.-S. Intercalation Chemistry of Graphite: Alkali Metal Ions and Beyond. *Chem. Soc. Rev.* **2019**, *48* (17), 4655–4687.

(4) Bhatt, M. D.; Lee, J. Y. High Capacity Conversion Anodes in Li-Ion Batteries: A Review. *Int. J. Hydrogen Energy* **2019**, *44* (21), 10852–10905.

(5) Yu, S.-H.; Feng, X.; Zhang, N.; Seok, J.; Abruña, H. D. Understanding Conversion-Type Electrodes for Lithium Rechargeable Batteries. *Acc. Chem. Res.* **2018**, *51* (2), 273–281.

(6) Jin, J.; Wu, L.; Huang, S.; Yan, M.; Wang, H.; Chen, L.; Hasan, T.; Li, Y.; Su, B.-L. Hierarchy Design in Metal Oxides as Anodes for Advanced Lithium-Ion Batteries. *Small Methods* **2018**, *2* (11), 1800171.

(7) Huang, B.; Pan, Z.; Su, X.; An, L. Tin-Based Materials as Versatile Anodes for Alkali (Earth)-Ion Batteries. *J. Power Sources* **2018**, *395*, 41–59.

(8) Guo, W.; Wang, Y.; Li, Q.; Wang, D.; Zhang, F.; Yang, Y.; Yu, Y. SnO2@C@VO2 Composite Hollow Nanospheres as an Anode Material for Lithium-Ion Batteries. *ACS Appl. Mater. Interfaces* **2018**, *10* (17), 14993–15000.

(9) Pedersen, A.; Khomyakov, P. A.; Luisier, M. Three-Phase Model for the Reversible Lithiation-Delithiation of SnO Anodes in Li-Ion Batteries. *Phys. Rev. Appl.* **2015**, *4* (3), 034005.

(10) Sensato, F. R.; Gracia, L.; Beltrán, A.; Andrés, J.; Longo, E. Structural and Electronic Properties of Lithiated SnO2. A Periodic DFT Study. *J. Phys. Chem. C* **2012**, *116* (30), 16127–16137.

(11) Li, J.; Wu, P.; Ye, Y.; Wang, H.; Zhou, Y.; Tang, Y.; Lu, T. Designed Synthesis of SnO2@C Yolk–Shell Spheres for High-Performance Lithium Storage. *CrystEngComm* **2014**, *16* (4), 517–521.

(12) Paek, S.-M.; Yoo, E.; Honma, I. Enhanced Cyclic Performance and Lithium Storage Capacity of SnO2/Graphene Nanoporous Electrodes with Three-Dimensionally Delaminated Flexible Structure. *Nano Lett.* **2009**, *9* (1), 72–75.

(13) Huang, J. Y.; Zhong, L.; Wang, C. M.; Sullivan, J. P.; Xu, W.; Zhang, L. Q.; Mao, S. X.; Hudak, N. S.; Liu, X. H.; Subramanian, A.; Fan, H.; Qi, L.; Kushima, A.; Li, J. In Situ Observation of the Electrochemical Lithiation of a Single SnO2 Nanowire Electrode. *Science* **2010**, *330* (6010), 1515–1520.

(14) Liu, H.; Long, D.; Liu, X.; Qiao, W.; Zhan, L.; Ling, L. Facile Synthesis and Superior Anodic Performance of Ultrafine SnO2-Containing Nanocomposites. *Electrochim. Acta* **2009**, *54* (24), 5782–5788.

(15) Zhang, W.-M.; Hu, J.-S.; Guo, Y.-G.; Zheng, S.-F.; Zhong, L.-S.; Song, W.-G.; Wan, L.-J. Tin-Nanoparticles Encapsulated in Elastic Hollow Carbon Spheres for High-Performance Anode Material in Lithium-Ion Batteries. *Adv. Mater.* **2008**, *20* (6), 1160–1165.

(16) Hong, Y. J.; Son, M. Y.; Kang, Y. C. One-Pot Facile Synthesis of Double-Shelled SnO2 Yolk-Shell-Structured Powders by Continuous

DOI: 10.1021/acsaem.9b01205
ACS Appl. Energy Mater. 2019, 2, 7244–7255

Process as Anode Materials for Li-Ion Batteries. *Adv. Mater.* **2013**, *25* (16), 2279−2283.
(17) Wang, J.; Li, W.; Wang, F.; Xia, Y.; Asiri, A. M.; Zhao, D. Controllable Synthesis of SnO2@C Yolk−Shell Nanospheres as a High-Performance Anode Material for Lithium Ion Batteries. *Nanoscale* **2014**, *6* (6), 3217−3222.
(18) Narsimulu, D.; Vadnala, S.; Srinadhu, E. S.; Satyanarayana, N. Electrospun Sn−SnO2/C Composite Nanofibers as an Anode Material for Lithium Battery Applications. *J. Mater. Sci.: Mater. Electron.* **2018**, *29* (13), 11117−11123.
(19) Liu, B.; Guo, Z. P.; Du, G.; Nuli, Y.; Hassan, M. F.; Jia, D. In Situ Synthesis of Ultra-Fine, Porous, Tin Oxide-Carbon Nanocomposites via a Molten Salt Method for Lithium-Ion Batteries. *J. Power Sources* **2010**, *195* (16), 5382−5386.
(20) Wang, H.; Oterkus, E.; Oterkus, S. Three-Dimensional Peridynamic Model for Predicting Fracture Evolution during the Lithiation Process. *Energies* **2018**, *11* (6), 1461.
(21) Zuo, P.; Zhao, Y.-P. Phase Field Modeling of Lithium Diffusion, Finite Deformation, Stress Evolution and Crack Propagation in Lithium Ion Battery. *Extreme Mechanics Letters* **2016**, *9*, 467−479.
(22) Galvez-Aranda, D. E.; Verma, A.; Hankins, K.; Seminario, J. M.; Mukherjee, P. P.; Balbuena, P. B. Chemical and Mechanical Degradation and Mitigation Strategies for Si Anodes. *J. Power Sources* **2019**, *419*, 208−218.
(23) Han, S.; Jang, B.; Kim, T.; Oh, S. M.; Hyeon, T. Simple Synthesis of Hollow Tin Dioxide Microspheres and Their Application to Lithium-Ion Battery Anodes. *Adv. Funct. Mater.* **2005**, *15* (11), 1845−1850.
(24) Lou, X. W.; Deng, D.; Lee, J. Y.; Archer, L. A. Preparation of SnO2/Carbon Composite Hollow Spheres and Their Lithium Storage Properties. *Chem. Mater.* **2008**, *20* (20), 6562−6566.
(25) Zeng, J.; Peng, C.; Wang, R.; Liu, Y.; Wang, X.; Liu, J. Large-Scale Synthesis of Hierarchical SnO Spheres Assisted with Poly (N-Isopropylacrylamide) for High Lithium Storage Capacity. *Ceram. Int.* **2019**, *45* (1), 1246−1250.
(26) Chang, P.-Y.; Doong, R. Microwave-Assisted Synthesis of SnO2/Mesoporous Carbon Core-Satellite Microspheres as Anode Material for High-Rate Lithium Ion Batteries. *J. Alloys Compd.* **2019**, *775*, 214−224.
(27) Yang, Z.; Du, G.; Feng, C.; Li, S.; Chen, Z.; Zhang, P.; Guo, Z.; Yu, X.; Chen, G.; Huang, S.; Liu, H. Synthesis of Uniform Polycrystalline Tin Dioxide Nanofibers and Electrochemical Application in Lithium-Ion Batteries. *Electrochim. Acta* **2010**, *55* (19), 5485−5491.
(28) Chen, S.; Wang, M.; Ye, J.; Cai, J.; Ma, Y.; Zhou, H.; Qi, L. Kinetics-Controlled Growth of Aligned Mesocrystalline SnO2 Nanorod Arrays for Lithium-Ion Batteries with Superior Rate Performance. *Nano Res.* **2013**, *6* (4), 243−252.
(29) Kong, Y.; Ma, Z.; Ye, Y.; He, G.; Sun, Y.; Zuo, X.; Xiao, X.; Nan, J. Nanosized Amorphous SnO2 Particles Anchored in the Wheat Straw Carbon Substrate as the Stabilized Anode Material of Lithium-Ion Batteries. *ACS Appl. Energy Mater.* **2018**, *1* (12), 7065−7075.
(30) Xu, Y.; Zhu, Y.; Liu, Y.; Wang, C. Electrochemical Performance of Porous Carbon/Tin Composite Anodes for Sodium-Ion and Lithium-Ion Batteries. *Adv. Energy Mater.* **2013**, *3* (1), 128−133.
(31) Gao, L.; Gu, C.; Ren, H.; Song, X.; Huang, J. Synthesis of Tin(IV) Oxide@reduced Graphene Oxide Nanocomposites with Superior Electrochemical Behaviors for Lithium-Ions Batteries. *Electrochim. Acta* **2018**, *290*, 72−81.
(32) Hu, R.; Chen, D.; Waller, G.; Ouyang, Y.; Chen, Y.; Zhao, B.; Rainwater, B.; Yang, C.; Zhu, M.; Liu, M. Dramatically Enhanced Reversibility of Li2O in SnO2-Based Electrodes: The Effect of Nanostructure on High Initial Reversible Capacity. *Energy Environ. Sci.* **2016**, *9* (2), 595−603.
(33) Kim, C.; Noh, M.; Choi, M.; Cho, J.; Park, B. Critical Size of a Nano SnO2 Electrode for Li-Secondary Battery. *Chem. Mater.* **2005**, *17* (12), 3297−3301.
(34) Ding, L.; He, S.; Miao, S.; Jorgensen, M. R.; Leubner, S.; Yan, C.; Hickey, S. G.; Eychmüller, A.; Xu, J.; Schmidt, O. G. Ultrasmall SnO_2 Nanocrystals: Hot-Bubbling Synthesis, Encapsulation in Carbon Layers and Applications in High Capacity Li-Ion Storage. *Sci. Rep.* **2015**, *4*, 4647.
(35) Deacon, P. R.; Mahon, M. F.; Molloy, K. C.; Waterfield, P. C. Synthesis and Characterisation of Tin(II) and Tin(IV) Citrates. *J. Chem. Soc., Dalton Trans.* **1997**, *0* (20), 3705−3712.
(36) Buqa, H.; Holzapfel, M.; Krumeich, F.; Veit, C.; Novák, P. Study of Styrene Butadiene Rubber and Sodium Methyl Cellulose as Binder for Negative Electrodes in Lithium-Ion Batteries. *J. Power Sources* **2006**, *161* (1), 617−622.
(37) Heubner, C.; Liebmann, T.; Voigt, K.; Weiser, M.; Matthey, B.; Junker, N.; Lämmel, C.; Schneider, M.; Michaelis, A. Scalable Fabrication of Nanostructured Tin Oxide Anodes for High-Energy Lithium-Ion Batteries. *ACS Appl. Mater. Interfaces* **2018**, *10* (32), 27019−27029.
(38) Shen, X.; Liu, H.; Cheng, X.-B.; Yan, C.; Huang, J.-Q. Beyond Lithium Ion Batteries: Higher Energy Density Battery Systems Based on Lithium Metal Anodes. *Energy Storage Materials* **2018**, *12*, 161−175.
(39) Hai, M.; Jun, M.; Jingyi, Q.; Zhongbao, Y.; Meng, L.; Junwei, Z. Lithium-Ion Full Batteries Based on the Anode of Non-Metallic Lithium. *Prog. Chem.* **2016**, *28* (2−3), 204−218.
(40) Padilla, R.; Sohn, H. Y. The Reduction of Stannic Oxide with Carbon. *Metall. Trans. B* **1979**, *10* (1), 109−115.
(41) Zhu, C.; Guo, S.; Fang, Y.; Dong, S. Reducing Sugar: New Functional Molecules for the Green Synthesis of Graphene Nanosheets. *ACS Nano* **2010**, *4* (4), 2429−2437.
(42) Mitchell, A. R.; Parker, R. H. The Reduction of SnO2 and Fe2O3 by Solid Carbon. *Miner. Eng.* **1988**, *1* (1), 53−66.
(43) Poizot, P.; Laruelle, S.; Grugeon, S.; Dupont, L.; Tarascon, J.-M. Nano-Sized Transition-Metal Oxides as Negative-Electrode Materials for Lithium-Ion Batteries. *Nature* **2000**, *407* (6803), 496.
(44) Stein, I. Y.; Constable, A. J.; Morales-Medina, N.; Sackier, C. V.; Devoe, M. E.; Vincent, H. M.; Wardle, B. L. Structure-Mechanical Property Relations of Non-Graphitizing Pyrolytic Carbon Synthesized at Low Temperatures. *Carbon* **2017**, *117*, 411−420.
(45) Ferrari, A. C. Raman Spectroscopy of Graphene and Graphite: Disorder, Electron−Phonon Coupling, Doping and Nonadiabatic Effects. *Solid State Commun.* **2007**, *143* (1), 47−57.
(46) Pimenta, M. A.; Dresselhaus, G.; Dresselhaus, M. S.; Cancado, L. G.; Jorio, A.; Saito, R. Studying Disorder in Graphite-Based Systems by Raman Spectroscopy. *Phys. Chem. Chem. Phys.* **2007**, *9* (11), 1276−1291.
(47) Ferrari, A. C.; Robertson, J. Interpretation of Raman Spectra of Disordered and Amorphous Carbon. *Phys. Rev. B: Condens. Matter Mater. Phys.* **2000**, *61* (20), 14095−14107.
(48) Park, M.-S.; Wang, G.-X.; Kang, Y.-M.; Wexler, D.; Dou, S.-X.; Liu, H.-K. Preparation and Electrochemical Properties of SnO2 Nanowires for Application in Lithium-Ion Batteries. *Angew. Chem., Int. Ed.* **2007**, *46* (5), 750−753.
(49) Kumar, P. P.; Yashonath, S. Ionic Conduction in the Solid State. *Proc. - Indian Acad. Sci., Chem. Sci.* **2006**, *118* (1), 135−154.
(50) Yashonath, S.; Ghorai, P. K. Diffusion in Nanoporous Phases: Size Dependence and Levitation Effect. *J. Phys. Chem. B* **2008**, *112* (3), 665−686.
(51) Lai, Y.; Wang, P.; Li, J.; Zhang, K.; Zhang, Z. Chemically Tailoring Porosity Carbon Foam with Oxygen-Containing Functional Groups to Restrain Polysulfide for Lithium-Sulfur Batteries. *J. Electroanal. Chem.* **2017**, *805*, 120−125.
(52) Zhang, S. S. Heteroatom-Doped Carbons: Synthesis, Chemistry and Application in Lithium/Sulphur Batteries. *Inorg. Chem. Front.* **2015**, *2* (12), 1059−1069.
(53) Zhang, L.; Wan, F.; Wang, X.; Cao, H.; Dai, X.; Niu, Z.; Wang, Y.; Chen, J. Dual-Functional Graphene Carbon as Polysulfide Trapper for High-Performance Lithium Sulfur Batteries. *ACS Appl. Mater. Interfaces* **2018**, *10* (6), 5594−5602.

DOI: 10.1021/acsaem.9b01205
ACS Appl. Energy Mater. 2019, 2, 7244−7255

(54) Zhao, X.; Luo, M.; Zhao, W.; Xu, R.; Liu, Y.; Shen, H. SnO2 Nanosheets Anchored on a 3D, Bicontinuous Electron and Ion Transport Carbon Network for High-Performance Sodium-Ion Batteries. *ACS Appl. Mater. Interfaces* **2018**, *10* (44), 38006−38014.
(55) Shimizu, M.; Yatsuzuka, R.; Koya, T.; Yamakami, T.; Arai, S. Tin Oxides as a Negative Electrode Material for Potassium-Ion Batteries. *ACS Appl. Energy Mater.* **2018**, *1* (12), 6865−6870.

DOI: 10.1021/acsaem.9b01205
ACS Appl. Energy Mater. 2019, 2, 7244−7255